


Measurements of velocity-selective resonances from adiabatic rapid passage

Yifan Fang, Edoardo Buonocore[✉], Michael Wahl[✉], and Harold Metcalf^{*}
Physics and Astronomy, Stony Brook University, Stony Brook, New York 11794-3800, USA

 (Received 11 January 2023; accepted 4 May 2023; published 17 May 2023)

Adiabatic Rapid Passage (ARP) allows the inversion of atomic states much faster than absorption–spontaneous-emission cycles with a concomitant large increase in momentum exchange rate and, hence, the applied optical forces. We have implemented ARP with appropriate modulators and polarizers on metastable He atoms on the $2^3S \rightarrow 2^3P$ transition at $\lambda \approx 1083.3$ nm. We have measured the velocity dependence of this force and have been surprised by the appearance of large peaks in the magnitude of this force at regularly spaced velocity intervals. Such unexpected behavior suggests that unexpected coherence effects come into play in optical forces, including those used for laser cooling.

DOI: [10.1103/PhysRevA.107.L051101](https://doi.org/10.1103/PhysRevA.107.L051101)

Introduction. Optical forces on atoms derive from the momentum exchange between them and an applied light field [1]. Atoms cannot absorb the linear momentum of light into their internal coordinates the same way as energy ($\Delta E \equiv \hbar\omega_\ell$) and angular momentum ($\Delta\ell = \pm 1$), so absorption or emission must involve atomic motion, usually in the form of a recoil momentum $\Delta E/c \equiv \hbar\omega_\ell/c \equiv \hbar k$. Since this is small compared to typical atomic momenta, it must be repeated many times to make a significant velocity change. Typically, an excitation is followed by a spontaneous emission and then repeated to achieve the multiple momentum exchanges. The rate γ of this process is limited by the excited state lifetime $\tau \equiv 1/\gamma$, so the maximum force scales with $\Delta p/\Delta t = \hbar k/\tau \equiv \hbar k\gamma$. In practice, excitation also takes time so this radiative force is given by $F_{\text{rad}} \equiv \hbar k\gamma/2$ for light tuned on resonance.

Here we describe our experiments that use adiabatic rapid passage (ARP) to compress both the excitation and the emission times and, thereby, strengthen the optical force to $F_{\text{ARP}} \gg F_{\text{rad}}$. The huge optical force enabled by multiple ARP sequences results from coherent exchange of momentum between atoms and light at a high repetition rate [2,3]. This is performed with counterpropagating pulses of frequency-swept light that alternately produce absorption followed by stimulated emission and has been demonstrated for atoms initially at rest [3]. The process falls into the category of “shortcuts to adiabaticity” that has become the subject of recent study [4].

An efficient pulse pair would leave an atom in its excited state $|e\rangle$ after the first pulse and its ground state $|g\rangle$ after the second pulse. This can be achieved with “ π pulses” [5–7], but such an approach is not very robust against variations in experimental conditions. By contrast, optical ARP [8–12] is a coherent control process that enables inversion and the concomitant momentum exchange in a way that is more resistant to experimental parameter variations. This has been demonstrated in our earlier work where we explored optical forces

based on ARP experimentally, analytically, and numerically [3,13–16].

The timing scheme for ARP-based absorption-stimulated emission cycles is illustrated in Fig. 1 where we denote the full cycle time by $4\pi/\omega_m$. Light from our cw lasers is both frequency swept and pulsed by EOM’s whose rf feeds are carefully synchronized. In all our experiments reported here, $\omega_m \approx 100\gamma \equiv 100/\tau \approx 2\pi \times 162$ MHz. A pulse of duration $\pi/\omega_m \approx 3.125$ ns from one direction (first pulse, e.g., from the left) is represented by the blue half-period sine wave in the upper trace, and its upward frequency sweep is represented by the corresponding first (blue) curve in the lower trace. A second pulse, incident from the opposite direction (e.g., from the right), is represented by the red second half-period sine wave, also with an upward frequency sweep (in this case). Thus, the momentum transfer is $2\hbar k$ in a time of $2\pi/\omega_m$, hence, the force without spontaneous emission is $F_{\text{ARP}} \equiv \hbar k\omega_m/\pi$ [17], and it can be orders of magnitude larger than the ordinary radiative force $F_{\text{rad}} \equiv \hbar k\gamma/2$.

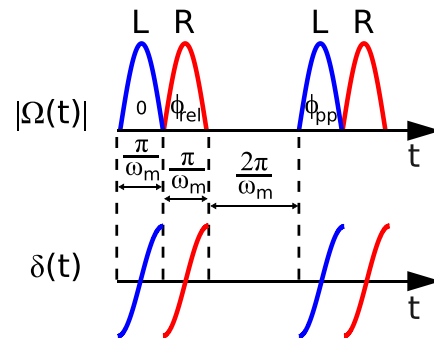


FIG. 1. The upper trace shows the Rabi frequency $\Omega(t)$ during a pulse pair, followed by the dead time and then the next pulse pair. The lower trace shows the frequency sweeps $\delta(t)$, in this case both upwards. The sweep time is $\pi/\omega_m \approx 3.125$ ns. Here ϕ_{pp} is the phase difference between the pulses arriving at the atom from opposite directions, and ϕ_{rel} is the phase shift of each laser pulse from its previous pulse. (Figure adapted from Ref. [3].)

^{*}Corresponding author: harold.metcalf@stonybrook.edu

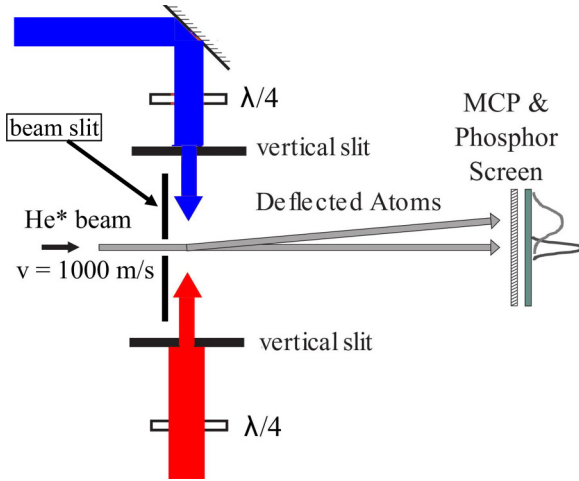


FIG. 2. A beam of metastable helium atoms (2^3S_1) enters from the left and is subject to counterpropagating laser pulses offset in time as shown in Fig. 1. The upper beam (blue) is first, and then the lower (red) comes next to make a pulse pair blue and red as in Fig. 1. Deflected atoms impinge on a spatially sensitive detector, whose image smeared by the longitudinal velocity distribution. The image is recorded and analyzed.

There is a dead time of $2\pi/\omega_m \approx 6.25$ ns between pulse pairs [3] to mitigate the effect of spontaneous emission, so the average expected force is $F_{\text{ARP}}/2$ without its deleterious effects. The ideal case has an atom in its ground state when the first pulse arrives. However, if the pulse sequence is interrupted by a spontaneous emission, an atom could be in its excited state when this first pulse arrives, thereby, reversing the force and reducing its average value. The dead time allows a bias toward decay before the first pulse, thereby, preferentially populating the ground state and correcting the error.

Experiments. The atomic beam part of our experiment is very similar to that of Ref. [3]. A beam of 2^3S_1 He atoms emerges from a DC discharge through a 0.5-mm aperture and is collimated by a vertical slit 250- μm wide 24 cm downstream. Atoms are deflected horizontally using pairs of counterpropagating laser pulses directed perpendicular to the atomic beam (see Fig. 2). The discharge also produces copious UV light resulting in an image of the slit on our detector and serves as a reference because it is not affected by our laser beams. We drive the transition $2^3S_1 \rightarrow 2^3P_2$ at $\lambda = 1083$ nm in neutral He atoms using diode lasers and fiber amplifiers. The width of each light beam determines a fixed atomic travel distance in the light, and its frequency sweep is tailored to apply the ARP force. The deflected atoms impinge on a spatially sensitive detector consisting of a microchannel plate and a phosphor screen assembly, and they are spread out transversely because of their longitudinal velocity distribution, as shown in Figs. 2 and 3. Their displacement is proportional to the force.

The image of the phosphor screen in Fig. 3(a) shows the UV light from a beam defined by the slit (vertical line spanning the whole image). The pulses are timed to push the atoms towards the left. The deflection seen on the microchannel plate is smeared because of the longitudinal velocity distribution of the atoms as shown in Fig. 2.

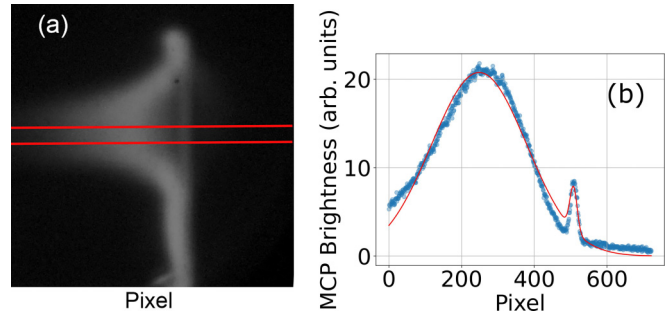


FIG. 3. An image of the phosphor screen is shown in part (a) with the pulses timed to push the atoms towards the left. The beam collimating slit (bright vertical line spanning the whole image) defines the position of UV light. In part (b), a line out of the atomic distribution between the thin horizontal (red) lines shows the relative flux of atoms vs detector position (slightly noisy plot). The line out is fitted with two Gaussians (smoother curve), one for the $v_a = 0$ marker near pixel 550, and the other for the displaced atoms. The fits for about 700 such images are all similar.

Among the parameters we can change is the frequency sweep direction of each of the pulses (see Fig. 1), and this produces four options for a pulse pair. Sweep directions can be up-up, up-down, down-up, and down-down. We have taken data with all four of these protocols, and the results are only slightly different. We can also vary the widths of the light beams so the atoms experience different numbers of pulse pairs. We have chosen 1.25-, 2.50-, and 3.73-mm-wide slits for our measurements. Within these 12 protocols, there are some variations from one data set to another, but these are small and there are many small effects that could cause such differences.

Velocity dependence of the force. An important criterion for a cooling force is a velocity dependence that is finite over some velocity range but vanishes at other velocities. Thus, atoms accumulate in the region of velocity space where the force is zero or very small so their velocity distribution is narrowed, and this constitutes cooling.

Atomic motion in the laboratory frame corresponds to Doppler-shifted frequencies in the atomic frame, so we oppositely detune the center frequency of the counterpropagating laser beams by $\delta = \pm kv_a$ to simulate the atomic velocity v_a in the vertical direction of Fig. 2 (horizontal in laboratory). This is indicated by the upward (red) and downward (blue) arrows. We lock one of our three Optica DL-100 lasers to the transition wavelength at 1083 nm using saturated absorption, and offset the other two by $\pm \delta$ to simulate a velocity $v_a = \pm \delta/k$ from it in the atomic rest frame. We have used this technique to measure the velocity dependence of the force over a range of simulated velocities.

For an ARP frequency sweep range of $\pm \delta_0$, one might expect a force capture range $|v_c| \sim (1/2)\delta_0/k$, and our measurements corroborate this. For most of our data we used $\delta_0 \approx 4.94 \omega_m = 2\pi \times 790$ MHz corresponding to $|v_c| \sim (1/2)\delta_0/k = 428$ m/s.

Presently we have no rigorous explanation for the peaks shown in Fig. 4, but offer the following heuristic model. Since the atoms have approximately uniform spatial distribution over thousands of wavelengths across the atomic beam, the

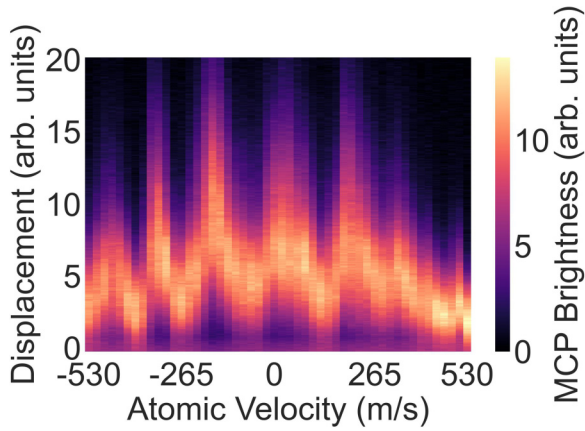


FIG. 4. Top view of about 55 data sets of the type in Fig. 3(b) plotted side-by-side (the UV peak is hidden just below the bottom). The vertical axis shows the “pixel” axis of Fig. 3(b) (reversed) so that larger displacements are upward, and the horizontal axis is for data taken at different “simulated” velocities v_a . The vertical axis of Fig. 3(b) (peak height) is indicated by color (brightness). The velocity v_a is calculated from the frequency offset of each laser δ using $v_a = \delta/k$. There are strong upward peaks that are periodically spaced in velocity. For these data, the peak Rabi frequency was $\Omega_0 \approx 3.36\omega_m$ and the sweep range was $\delta_0 \approx \pm 4.94\omega_m$.

two pulses of the first pulse pair could have a different phase for different atoms. Then, the next pulse pair could arrive with the atoms at various places because of their different initial transverse velocities, and, thus, with completely different phases, except for atoms that have moved an integer number of wavelengths between pulse pairs.

Since the necessary feature of our multiple ARP processes is that the Bloch vector’s motion on the Bloch sphere should not be discontinuously interrupted by any sharp phase changes, atoms that have moved an integer number of wavelengths experience the same pulse-to-pulse phase (see ϕ_{pp} of Fig. 1) and, thus, consistently larger forces. Such atoms travel $v_a \times 6.25$ ns between pulse pairs which is $n\lambda$ for $v_a = n \times 173$ m/s. This is consistent with our Fourier transform in Fig. 5(b) below.

Data analysis. In our experiments, the interaction time between atoms and light is determined by the width of the light beam traversed by the atoms, and we can vary this with slits for each beam that define its width and block the Gaussian tails of the beam profiles. To minimize the effects of slit diffraction, we image the slits 1:1 onto the atomic beam. Most of our data is taken with 3.75-mm slits corresponding to an average interaction time of ≈ 3.6 μ s, but the width of the longitudinal velocity distribution broadens this considerably. It is centered at ~ 1050 m/s, has a full width at half maximum of about 400 m/s and is slightly asymmetric. This corresponds to ~ 300 pulse pairs since the dead time for each pair is another ≈ 6.25 ns, making an ≈ 12.5 ns/pulse pair as in Fig. 1.

We have separated our data by interaction time (slit width) and compared the three data sets using 1.25-, 2.50-, and 3.75-mm width slits. The peak height distribution of Fig. 5(a) are all very similar showing no significant dependence on interaction time. The velocity resonances appear over a range

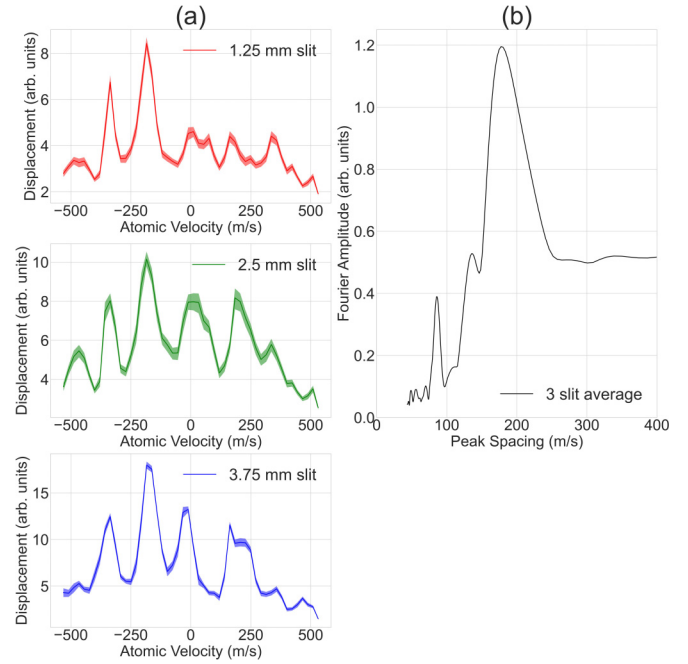


FIG. 5. Part (a) shows these peak heights for various slit widths (interaction time). All of these data were taken on different days over a period of several weeks. The resonances show up clearly and are all quite similar. Each of these has been Fourier transformed, and the three transforms were averaged. Then, the horizontal axis was transformed to v_a instead of the conjugate $1/v_a$ as shown in part (b).

of interaction times with about the same spacing and widths. They are typically twice as high as the average force in the region between them.

The Gaussian fits to ~ 700 data sets exemplified by Figs. 3 and 4 are good enough to extract a reliable peak (centroid) from each. The UV peak provides a $v_a = 0$ marker for the measurements for atoms. We have plotted the height of these peaks vs v_a in Fig. 5(a) and their Fourier transform in Fig. 5(b). The Fourier transform peaks at 177 ± 5 m/s, consistent with the 173 m/s calculated above. The velocity range of these data span $\sim \pm 500$ m/s, as expected. The peaks on some of the plots are offset from center, and we attribute this to slight misalignment of the laser beams from perpendicular to the atomic beam. Since the average longitudinal velocity is 1050 m/s, a 1° misalignment causes a velocity offset of 18 m/s.

We have many data sets with slit widths between 1.25 and 3.75 mm, but the net displacement of atoms does not vary linearly with the slit width that corresponds to the number of pulse pairs that hit the atoms (the atomic displacement for slits smaller than 1.25 mm is too hard to measure). We attribute this nonlinearity to the Doppler detuning arising from the change in atomic velocity during the interaction time. For example, 200 pulse pairs changes the speed by $200 \times 2v_{\text{recoil}} \approx 36$ m/s, resulting in a Doppler shift of ~ 33 MHz. The average Rabi frequency during a pulse is $(2/\pi)\Omega_0 \sim 2 \times \omega_m \sim 2\pi \times 320$ MHz so this Doppler shift is about 10% of the power-broadened width. This is not large, but we estimate that it is enough to account for this deviation from linearity. This estimate could be substantiated if we could

measure atomic displacements using a slit width less than 1.25 mm.

Summary. Since the advent of laser cooling in the 1980s, there have been many studies of increases in the strength of optical forces beyond the monochromatic radiative force $F_{\text{rad}} \equiv \hbar k \gamma / 2$. In the experiments reported here, we have used the atomic displacement and interaction time to calculate the measured optical force on the atoms, and we used these results to measure the velocity dependence of $F_{\text{ARP}} \gg F_{\text{rad}}$. Moreover, we found the effective velocity range is much larger than that of F_{rad} . What has surprised us most is the appearance of multiple resonances of the forces at velocities corresponding to atomic travel of an integer number of wavelengths during the 6-ns pulse cycles. These are strong and robust as shown in our data. The laser setup enables further exploration of the dependence of the ARP force on v_a as well as the role of phase noise that can be inserted experimentally. We expect that this will lead to further understanding of the role of coherence in multifrequency forces and provide a clearer understanding of shortcuts to adiabaticity.

In addition, we are working on a numerical simulation of this experiment using the optical Bloch equations in the Lindblad formalism to include spontaneous emission [18]. We extract the time dependence of the solutions and calculate the force on the atoms from the w component of the resulting Bloch vector. We calculate the positions of the atoms after their flight from the interaction region to the detector (see Fig. 2). These show the velocity-dependent structures for a few pulse pairs, but our experiments use hundreds of pulse pairs. The eventual results will be published separately. We hope that it will unravel some of the puzzles we have observed in these preliminary measurements.

We are also working on a scheme of improved velocimetry to avoid the effect of the spreading from the atomic beam's longitudinal velocity distribution.

Acknowledgments. We are grateful to B. Arnold for his substantial contribution in the earliest days of this project. We also wish to thank M. G. Cohen, O. Nicholson, I. Schwartz, and E. Jones. Finally, we acknowledge financial support from the Office of Naval Research.

-
- [1] H. Metcalf and P. v. d. Straten, *Laser Cooling and Trapping* (Springer Verlag, New York, 1999).
 - [2] H. Metcalf, Strong optical forces on atoms in multifrequency light, *Rev. Mod. Phys.* **89**, 041001 (2017).
 - [3] X. Miao, E. Wertz, M. G. Cohen, and H. Metcalf, Strong optical forces from adiabatic rapid passage, *Phys. Rev. A* **75**, 011402(R) (2007).
 - [4] D. Guéry-Odelin, A. Ruschhaupt, A. Kiely, S. Martinez-Garaot, and J. G. Muga, Shortcuts to adiabaticity: Concepts, methods, and applications, *Rev. Mod. Phys.* **91**, 045001 (2019).
 - [5] L. Allen and J. H. Eberly, *Optical Resonance and Two-Level Atoms* (Dover, New York, 1987).
 - [6] A. Goepfert, I. Bloch, D. Haubrich, F. Lison, R. Schütze, R. Wynands, and D. Meschede, Stimulated focusing and deflection of an atomic beam using picosecond laser pulses, *Phys. Rev. A* **56**, R3354(R) (1997).
 - [7] P. Berman and V. Malinovsky, *Principles of Laser Spectroscopy and Quantum Optics* (Princeton University Press, Princeton, New Jersey, 2011).
 - [8] M. M. T. Loy, Observation of Population Inversion by Optical Adiabatic Rapid Passage, *Phys. Rev. Lett.* **32**, 814 (1974).
 - [9] L. P. Yatsenko, S. Guérin, and H. R. Jauslin, Topology of adiabatic passage, *Phys. Rev. A* **65**, 043407 (2002).
 - [10] M. A. Norcia, J. R. K. Cline, J. P. Bartolotta, M. J. Holland, and J. K. Thompson, Narrow-line laser cooling by adiabatic transfer, *New J. Phys.* **20**, 023021 (2018).
 - [11] J. P. Bartolotta, M. A. Norcia, J. R. K. Cline, J. K. Thompson, and M. J. Holland, Laser cooling by sawtooth-wave adiabatic passage, *Phys. Rev. A* **98**, 023404 (2018).
 - [12] J. P. Bartolotta and M. J. Holland, Sawtooth-wave adiabatic passage in a magneto-optical trap, *Phys. Rev. A* **101**, 053434 (2020).
 - [13] T. Lu, X. Miao, and H. Metcalf, The Bloch theorem on the Bloch sphere, *Phys. Rev. A* **71**, 061405(R) (2005).
 - [14] X. Miao, Optical force on atoms with periodic adiabatic rapid passage sequences, Ph.D. thesis, Stony Brook University, 2006.
 - [15] T. Lu, X. Miao, and H. Metcalf, Non-adiabatic transitions in adiabatic rapid passage, *Phys. Rev. A* **75**, 063422 (2007).
 - [16] D. Stack, J. Elgin, P. M. Anisimov, and H. Metcalf, Numerical studies of optical forces from adiabatic rapid passage, *Phys. Rev. A* **84**, 013420 (2011).
 - [17] This is the same definition as that in Refs. [13,15] but different from that of Ref. [3].
 - [18] P. Meystre, *Quantum Optics: Taming the Quantum* (Springer, Berlin, New York, 2021).